Mechanical characterisation of a viscoplastic material sensitive to hydrostatic pressure

Michel Gratton, Camille Gontier, Saïd Rja Fi Allah, Abdelhake Bouchou, Didier Picart

Mechanical characterisation of a viscoplastic material sensitive to hydrostatic pressure

Michel Gratton, Camille Gontier, Saïd Rja Fi Allah,
Abdelhake Bouchou, Didier Picart

PII: S0997-7538(09)00034-5
DOI: 10.1016/j.euromechsol.2009.03.002
Reference: EJMSOL 2510

To appear in: *European Journal of Mechanics A/Solids*

Received date: 21 December 2007
Accepted date: 11 March 2009

Please cite this article as: M. Gratton, C. Gontier, S. Rja Fi Allah, A. Bouchou, D. Picart, Mechanical characterisation of a viscoplastic material sensitive to hydrostatic pressure, *European Journal of Mechanics A/Solids* (2009), doi: 10.1016/j.euromechsol.2009.03.002

Paper submitted to
EUROPEAN JOURNAL OF MECHANICS - A/SOLIDS

First submission: December 21, 2007
First revision: October 10, 2008
Second revision: March 10, 2009

Title:
Mechanical characterisation of a viscoplastic material sensitive to hydrostatic pressure

Authors:
Michel GRATTON *, Camille GONTIER*, Saïd RJA FI ALLAH*, Abdelhake BOUCHOU[*], Didier PICART**

[*]*Ecole Nationale d'Ingénieurs du Val de Loire, Blois, France, Laboratoire de Mécanique et Rhéologie, EA 2640, Université François Rabelais, Tours, France*
[**]*C.E.A. Le Ripault , Monts, France*

30 pages, 1 table, 12 figures,

Corresponding author:

Professor Camille GONTIER, Ecole Nationale d'Ingénieurs du Val de Loire, Rue de la Chocolaterie, BP 3410, 41034 Blois Cedex, France. Tel. 33 (0)2 54 55 84 05, Fax: 33 (0)2 54 55 84 41, e-mail: camille.gontier@univ-tours.fr

Co-authors:

Doctor Michel GRATTON, Ecole Nationale d'Ingénieurs du Val de Loire, Rue de la Chocolaterie, BP 3410, 41034 Blois Cedex, France. Tel. 33 (0)2 54 55 84 21, Fax: 33 (0)2 54 55 84 41, e-mail: michel.gratton@univ-tours.fr

Saïd RJA FI ALLAH, Ecole Nationale d'Ingénieurs du Val de Loire, Rue de la Chocolaterie, BP 3410, 41034 Blois Cedex, France. Tel. 33 (0)2 54 55 84 11, Fax: 33 (0)2 54 55 84 41, e-mail:said.rjafiallah@univ-tours.fr

Doctor Abdelhake BOUCHOU, Ecole Nationale d'Ingénieurs du Val de Loire, Rue de la Chocolaterie, BP 3410, 41034 Blois Cedex, France, Tel. 33 (0)2 54 55 84 23, Fax: 33 (0)2 54 55 84 41, e-mail: abouchou@univ-tours.fr

Doctor Didier PICART, C.E.A. Le Ripault , BP 16, 37260 Monts, France. Tel. 33 (0)2 47 34 41 73, e-mail: didier.picart@cea.fr

Mechanical characterisation of a viscoplastic material sensitive to hydrostatic pressure

Michel GRATTON , Camille GONTIER, Saïd RJA FI ALLAH, Abdelhake BOUCHOU
Ecole Nationale d'Ingénieurs du Val de Loire, Laboratoire de Mécanique et Rhéologie, Blois, France
and
***Didier PICART**, C.E.A. Le Ripault , Monts, France*

Abstract

The present paper deals with the characterisation of the static mechanical behaviour of an energetic material all along its lifespan. The material behaviour is viscoplastic, damageable and sensitive to hydrostatic pressure. For such materials, existing models have generally been developed in the framework of transient dynamic behaviour. These models are not suitable for a static study. Therefore a specific experimental protocol and an associated model are developed. Characterisation is derived from both uniaxial compressive, tensile tests and tri-axial tests. Plastic behaviour is described by means of a parabolic yield criterion and a new hardening law. Non-associated plastic flow rule and isotropic damage complete the model. The performance of the model is illustrated through the simulation of various loading paths.

Keywords: Mechanics, Material, Modelling, Viscoplasticity, Damage

Symbols

$E,\ \nu$ Elastic modulus, elastic Poisson ratio

$\boldsymbol{\varepsilon}, \boldsymbol{\varepsilon_e}, \boldsymbol{\varepsilon_p}$, total, elastic, plastic deformation tensors

$\boldsymbol{\sigma}, \boldsymbol{\sigma^D}$ total and deviatoric stress tensors

P, τ volumic and octaedric stresses

f, *k* yield function and strain hardening parameter

$\varepsilon_p^v, \varepsilon_p^D$ volumetric and deviatoric plastic strains

p effective plastic strain

β, $\boldsymbol{n}$ dilatancy and flow direction

d damage factor

1. Introduction

The material studied is made of 94% energetic Octogen cristals (octahydro-1,3,5,7-tetranitro-1,3,5,7-tetrazocine, HMX), polydispersed from 0,1 up to 600µm, and mixed with around a 4% heat-hardening binder. After an isostatic compaction forming process, the global residual porosity is estimated at 2%. A concrete-like material is obtained, with the largest grains embedded in a "matrix" including the binder, the smallest crystals and most of the porosity. A lot of micro-cracks are present inside or between the crystals.

It turns out that all along its lifespan, the mechanical properties of the material must be continuously and closely observed. To this end a periodic sampling is performed among the quantity available but only a small amount of material can be taken off at each stage. Nevertheless, the material needs to be characterised accurately in terms of viscoplastic behaviour and damage effects. This characterisation must be derived from a reduced number of standard tests. Taking these constraints into account, an experimental procedure based on a reduced number of tests has been defined. This procedure provides a numerical dataset from which the material characteristics must be drawn.

The samples are cut off in cylindrical or prismatic shapes of various dimensions. In any case the sample volume is large compared to the typical dimension of its granular components. It is assumed that the selected tests are representative with respect to the current uses of the material. This means that the mechanical model must fit accurately the data available, and reproduce some typical tests in the field of application.

Fig. 1 shows the curves obtained from three typical loading programs: a longitudinal cyclic compressive test, a tri-axial cyclic compressive test with 10 MPa initial hydrostatic pressure and a cyclic tensile test. The observation of the curves immediately shows some main features of the material, and entails specific arrangements for the mechanical tests. 1) Temperature: although in its usual applications, the material lies far from its glass transition, its behaviour remains temperature-dependent. In the first approach this influence is out of the scope of the study, therefore all tests are performed at a constant 20° C room temperature. 2) Hydrostatic pressure sensitivity: the high volume fraction of the granular phase reveals both the differences between compressive and tensile experiments, and the behavior observed at higher hydrostatic pressures (Wiegand, 1999) (Wiegand, Reddingius, 2004). This factor is highly relevant to the material plastic behaviour. To take this into account the compressive tests first include a hydrostatic loading phase (0 MPa, 5 MPa, 10 MPa) followed by a longitudinal compressive phase. 3) Viscous effects: for compressive and tensile

tests, a dependence on the strain rate and on the temperature is observed (D.J. Funk et al, 1995) (Idar et al, 2001), even for a low polymer fraction (approx. 5%wt). Furthurmore, a series of tests at different strain rates ($5.10^{-6}s^{-1}$ to $10^{-3}s^{-1}$) confirms the presence of such effects. A viscoplastic behaviour is assumed while the visco-elasticity is neglected. To capture the viscous and hardening parameters, relaxation delays are introduced at the end of each loading phase. 4) Dispersion: to ensure a minimum statistical validity, each loading program is repeated several times. However, because of the material constraints mentioned above, this number is restricted to five. 5) Initial elastic parameters: standard tests in various material directions confirm that these parameters are almost isotropic. 6) Damage: to capture this information, systematic cyclic loading-unloading programs are performed. In fact, the tests show increasing anisotropy during loading. For the sake of simplicity, the isotropic damage is assumed. Slight differences are thus expected between a real cyclic program and its modelling, especially for the last cycles.

Earlier modelling approaches for such materials (Addessio and Johnson, 1990), (Bennett et al., 1998), (Hackett and Bennett, 2000) have been developed in the framework of transient dynamic behaviour, thus are not suitable for a static study. So a new model and the associated experimental protocol are developed. To summarise, the model assumes an elastoplastic damageable behaviour with hydrostatic pressure sensitivity, constant isotropy all along the loading path and no coupling between viscoplasticity and damage.

2. Test procedure

Cylindrical 10 mm radius, 20 mm high samples are used for compressive tests, and 150 mm long dumbbell samples for tensile tests. A 100 kN hydraulic machine is used to apply, control and record strains and stresses along complex loading paths.

The samples are fitted with opposite pairs of strain gauges which allow an estimation of the test quality and provide averaged longitudinal and lateral strains. Stresses are derived from the axial force applied by the machine. A hydrostatic pressure can be applied to the sample, and the additive stress is directly given by the water pressure.

As mentioned above, the experimental data set results from a series of loading programs for different initial hydrostatic pressure values. The hydrostatic pressure is first applied and then a longitudinal cyclic load is added up to rupture. Tensile tests are performed without hydrostatic pressure. The machine is driven by controlling the mean strain of the longitudinal gauges.

Fig. 2 gives an example of the curves which are extracted from a typical test, here the cyclic compressive test with 5 MPa initial hydrostatic pressure. Segment OA_1 represents the elastic hydrostatic loading phase. Then a sequence of 5 to 6 loading-relaxation-unloading cycles is performed. A typical loop $A_iB_iC_iA_{i+1}$ is enhanced on the figure. Relaxation delays have been defined from preliminary experiments to guarantee an almost complete relaxation of viscous stresses. From these observations it has been established that a 15-minute relaxation time for the first three cycles and a 60-minute relaxation time for further ones is sufficient. From these figures, the following information is picked up:

- At point C_i couple (ε,σ) defines a point of the current yield surface.

- Slope (E) of line $A_{i+1}C_i$ defines the current elastic modulus.

- Segment $A_{i+1}G_{i+1}$ whose slope is E/(1-2ν), and which represents the hydrostatic pressure unloading, defines plastic strain $\varepsilon_p = \overline{OG_{i+1}}$. Assuming the bulk modulus constant, it results in:

$\varepsilon_p = \overline{A_1A_{i+1}}$.

As a matter of fact, similar information can be drawn simultaneously from the longitudinal and from the transverse strain records, as shown by fig. 1 and 2.

3. Yield criterion and hardening law

A survey on the most famous criteria of isotropic plasticity can be found in literature (Aubertin and Li, 2004). A specific criterion known as “Cam-clay” model (Prevost and Popescu, 1996), bounded in all stress directions, was early developed at Cambridge University with a view to modelling soils. Numerous versions were further developed for various applications (Coussy 1995), (Gontier et al., 2001), (Hicher and Shao, 2008), also based on closed criteria. These models are not suitable for some materials, which require an open criterion in the negative stress direction. For such materials better models generally derived from earlier formulations - Mohr-Coulomb, Mises-Schlecher (Schleicher 1996) and Drucker-Prager (Drucker *et al*., 1957) - were proposed then extensively applied (Pan and Hudson, 1988). A unified model has recently been proposed (Aubertin and Li, 2004), allowing elliptic, parabolic or hyperbolic criteria, and including the notion of Lode’s angle which expresses the influence of the third stress invariant. An application of Mises-Schlecher’s criterion to polymers has been developed (Raghava et al., 1973), where two hardening variables respectively associated with tensile and compressive responses are introduced.

Assuming a small deformation hypothesis the total strain can be partitioned into two parts: a

reversible elastic strain and a permanent plastic one: $\boldsymbol{\varepsilon} = \boldsymbol{\varepsilon}_e + \boldsymbol{\varepsilon}_p$ (3.1)

Moreover, assuming the isotropy hypothesis, the constitutive equations can be expressed in terms of stress and strain tensor invariants: volumic stress, volumetric strain, octaedric stress and strain, etc.

3.1. The yield criterion

The material is produced under a 200 MPa compaction phase, which is largely above the maximum stress used. Consequently the yield criterion must be open in the negative *P* direction.

The yield surface that bounds the elastic-domain can be defined in (P, τ) coordinates, τ being the octaedric stress and *P* the volumic stress, defined as:

$$P = Tr(\boldsymbol{\sigma})/3 \qquad \tau = \sqrt{1/3\, \boldsymbol{\sigma}^D : \boldsymbol{\sigma}^D} \qquad \text{(3.2 a, b)}$$

where $\boldsymbol{\sigma}$ is the current stress tensor and $\boldsymbol{\sigma}^D$ its deviator. A parabolic criterion, which was recently used by several authors (Winnicki et al., 2001) for concrete modelling, meets the requirement of a semi-opened yield surface. Generally, such a criterion includes two hardening parameters f_c and f_t in order to represent the evolution of the limit curve along the tensile directions (f_t) and the compressive directions (f_c).

$$f = \frac{3}{2}\boldsymbol{\sigma}^D : \boldsymbol{\sigma}^D + P(f_c - f_t) - f_c f_t = 0 \qquad (3.3)$$

The model proposed hereafter uses a unique hardening parameter *k* covering both tensile and compressive tests: $f = \sqrt{\tau^2 + b(k)\,P} - k = 0$ (3.4)

where *b*(*k*) is a function which is defined below.

For *P* = 0, the solution of equ. (3.4) is $\tau\big|_{f=0,P=0} = k$ which means that *k* locates the intersections of the yield curve with the τ axis (fig. 3). For τ = 0, the solution $P\big|_{f=0,\tau=0}$ to equ. (3.4) defines a function $X(k) = \frac{k^2}{b(k)}$ which locates the summit of the parabola on the *P* axis. To summarise, a yield curve can be defined by pair $(k, X(k))$ defining its intersections with the axes. The initial yield curve is defined by pair (k_0, X_0) and the extreme yield curve by pair (k_m, X_m). The current yield curve equation is then:

$$f(\tau, P, k) = \sqrt{\tau^2 + \frac{k^2}{X(k)}P} - k = 0 \qquad (3.5)$$

and the set of yield curves is completely defined as soon as function $X(k)$ and the hardening law are defined.

The choice of function $X(k)$, or equivalently $b(k)$ is crucial in view of the model accuracy, and depends on fundamental hypotheses.

First it is assumed that the yield curves do not cross each other in the (P,τ) plane, each one being embedded in those of higher levels, and all of them being embedded in the extreme curve. This is a strong hypothesis which is generally associated with the hypothesis of isotropic strain-hardening. The consequence is that at some point of the (P,τ) plane, no more than one yield curve passes. In the present case, this ensures that for any loading process, the more the yield stress increases the more strain-hardening parameter k increases. Fundamentally, this is a necessary - but not sufficient - condition for the strain-hardening phenomenon to be governed by a unique state variable which is the strain-hardening parameter.

The simplest formulation $b(k)$=Cste was immediately rejected because it could not represent the progressive growing of the elastic domain. More complex hypotheses, such as $b(k)$ depending on some deformation parameters (Shao et al, 2006), were tried but generally led to yield curves crossing each other in the (P,τ) plane. Finally the simplest choice of a linear function $X(k)$ proved to avoid these drawbacks and sufficient to meet all the major conditions, without any final advantage of a more complex expression. Moreover, the comparison of a monotonous loading path and a more complex triaxial loading path showed the consistency of the model.

Elementary algebra shows that two curves (3.5) defined by pairs (k_1, X_1) and (k_2, X_2), with $k_2>k_1$, do not intersect in the (P,τ) plane if : $\frac{X_2}{k_2^2} < \frac{X_1}{k_1^2}$. Therefore the embedding condition of the yield curves is that function $\frac{X(k)}{k^2}$ is a monotonous decreasing function of k.

Assuming that the two pairs (k_0, X_0) and (k_m, X_m) are known, the most simple expression of $X(k)$ is a linear relation fitted onto these two pairs, thus:

$$X = X_0 + (X_m - X_0)\frac{k - k_0}{k_m - k_0} \tag{3.6}$$

From this choice, it is easy to prove that function $\frac{X(k)}{k^2}$ is monotonously decreasing if the following condition is met:

$$k_m X_0 - k_0 X_m > 0 \tag{3.7}$$

Therefore, pairs (k_0, X_0) and (k_m, X_m), and a hardening law in order to relate parameter k to the

plastic strain history of the material need to be determined.

On fig. 3 the yield points extracted from the data set are represented for the whole experimental program. For all compressive tests, the last loading cycle before fracture (fig. 2) shows a horizontal part which can be interpreted as a hardening limit. Tensile tests present a brittle fracture (fig. 1) at low stresses when the yield surface has not been reached. Consequently only compressive tests are used to define the ultimate yield surface. This surface can be determined by fitting a parabola on points B_n (fig. 3) through a least-squares procedure, which determines the values of X_m and k_m at its intersections with the axes.

The determination of pair (X_0, k_0) is more puzzling since the elastic bound cannot be clearly located on the loading curves, except within an approximate band in the plane (fig. 3). It results that pair (X_0, k_0) should be better determined by means of a global optimisation of the hardening law, which is the subject of the next section.

Pairs (k_0, X_0), (k_m, X_m) being determined, equ. (3.5) and (3.6) define a family of non-intersecting yield curves provided that the condition (3.7) is met.

3.2. Strain-hardening law

To define a strain-hardening rule, relationship $k(p)$ must be established linking hardening parameter k to some state variable p featuring the cumulated history of the plastic strain.
Variable p and mathematical relation $k(p)$ must be chosen so that all the experimental loading programs generate a unique curve $k(p)$ in the (k, p) plane. At first glance, the plastic deviatoric strain seems suitable for variable p but simple calculations show that a unique curve $k(p)$ cannot be obtained from this choice, and that the volumetric plastic strain is involved in the model. Defining two quantities $\dot{\varepsilon}_p^v$ and $\dot{\varepsilon}_p^D$ respectively as the volumetric and the deviatoric plastic strain rates:

$$\dot{\varepsilon}_p^v = Tr(\dot{\boldsymbol{\varepsilon}}_p) \quad ; \qquad \dot{\varepsilon}_p^D = \sqrt{3\,\dot{\boldsymbol{\varepsilon}}_p^D : \dot{\boldsymbol{\varepsilon}}_p^D} \tag{3.8 a, b}$$

a combination of these two factors, hereafter labelled "effective strain" is proposed, as in (Nova, 1982), i.e. in incremental form:

$$\dot{p} = \delta\ \dot{\varepsilon}_p^v + (1-\delta)\ \dot{\varepsilon}_p^D \tag{3.9 a}$$

where δ is a constant parameter in the [0-1] range, bounded by the value which ensures that the effective strain continuously increases. Actually, the quantities defined by eq. (3.8) are related through a fundamental

parameter called "dilatancy' β attached to current state (p, P), so that eq. (3.9 a) can be written as:

$$\dot{p} = \delta\ \dot{\varepsilon}_p^v + (1-\delta)\ \dot{\varepsilon}_p^D = \Big(1+\delta\big(\beta(P,p)-1\big)\Big)\dot{\varepsilon}_p^D \qquad (3.9\text{ b})$$

The intoduction of parameter δ lies on the statement that an increase on pure hydrostatic pressure necessarily involves an increase on the hardening parameter. From another point of view, parameter δ is used to gather all the loading curves onto a unique curve in the (P,τ) plane. The meaning of this strategy is to give sense to the notion of strain hardening as a fundamental state of the material.

The form of the hardening law includes three parameters k_0, c_1, c_2, which are necessary to control elastic limit k_0, initial hardening modulus $c_1(k_m - k_0)$ and the global curvature. A hyperbolic form is thus proposed:

$$k = k_0 + (k_m - k_0)\left(1 - \frac{1}{1 + c_1\, p + c_2\, p^2}\right) \qquad (3.10)$$

The form of this expression was chosen to fit accurately the shape of the hardening curves. A hyperbolic form provides the nearly asymptotic behaviour while complementary term $c_2\, p^2$ allows some control on the initial slope.

Yield equations (3.5), (3.6), effective strain definition (3.8) together with strain-hardening relation (3.10) completely define the family of yield surfaces.

3.3. Characterisation of the criterion and hardening law parameters

In these equations the set of parameters X_0, k_0, δ, c_1, c_2 must be fitted so that implicit function $k(p)$ makes the loading paths gather around a unique curve as accurately as possible. Firstly the coefficients are approximated by hand. Coefficients X_m and k_m are first determined by using the yield points on the loading curves. Then the 3 parameters X_0, k_0, δ are fitted so as to gather the hardening curves onto a unique curve. Finally, parameters c_1, c_2 are determined so as to ensure the correct shape of this curve.

From this initial parameter set, a global optimisation procedure (see Appendix A1.1) is applied to improve the consistency of the model, leading to slightly different parameters. The procedure uses a simple gradient method. Some difficulty stems from the fact that variables X_0, k_0, k are linked through implicit relations (3.5) (3.6). Appendix A1.1 summarises the mathematical calculations.

The coefficients which result from this procedure are X_0 = 1.5 MPa, X_m = 1.62 MPa, k_0 = 0.26 MPa, k_m = 3.35 MPa, δ = 0.6796 MPa, c_1 = 1400 MPa, c_2 = 80000 MPa. With these values

condition (3.7) is met.

Fig. 4 shows the superposition of the loading programs in the (k, p) plane, together with the mean curve resulting from the parameter optimisation. Fig. 5 shows the family of yield curves obtained in the (P,τ) plane from the previous model.

4. Viscoplastic flow rule

The plastic flow rule is defined in two steps. Given $\dot{\boldsymbol{\varepsilon}}_{\boldsymbol{p}} = \dot{\lambda}\boldsymbol{n}$, plastic flow direction $\boldsymbol{n}$ then plastic strain rate $\dot{\lambda}$ along this direction are successively determined.

4.1. Viscoplastic flow direction

Flow direction $\boldsymbol{n}$ can be established from experimental data by considering quotient β between the volumetric and deviatoric plastic strain rates, usually called "dilatancy". $$\beta = \frac{\dot{\varepsilon}_p^v}{\dot{\varepsilon}_p^D} \tag{4.1}$$

From this value, the flow direction $\boldsymbol{n}$ at that point, normalised in the sense that $\boldsymbol{n}:\boldsymbol{n}=1$, is given by:

$$\boldsymbol{n} = \frac{1}{\sqrt{3(1+\beta^2)}}\left(\frac{\boldsymbol{\sigma}^{\boldsymbol{D}}}{\tau} + \beta\mathbf{I}\right) \tag{4.2}$$

Proof is given in appendix A2.

The flow model to be developed expresses the flow direction as a function of the current state variables. On fig. 5 the flow directions are indicated by arrows at all experimental points of the yield curves. Since these arrows are not orthogonal to the yield curves, the material does not follow the standard "associated plasticity" law. A classical approach consists in determining a function g called "plastic potential" from which the flow direction is derived: $$\dot{\boldsymbol{\varepsilon}}_{\boldsymbol{p}} = \dot{\lambda}\frac{\partial g}{\partial \boldsymbol{\sigma}} \tag{4.3}$$

Another method is to fit directly a simple mathematical model onto the set of experimental flow directions following a few heuristic guidelines. Once more it is assumed that at some point of the (P,τ) plane, the flow direction is unique. Fundamentally this hypothesis means that the representation of the flow rule does not require anymore state parameter than those defined above. It results that dilatancy β can be defined as a function of pair (p, P) alone.

Defining the angular position of the flow direction in the (P,τ) plane by $\frac{\pi}{2}-\theta$, with

$$\theta = \arctan(\beta) \tag{4.4}$$

the aspect of the potential curves, which must necessarily be convex, suggests that θ must be a monotonous increasing function of p when P is constant and also of P when p is constant. The smallest number of parameters should be 3, allowing a linear representation $\theta = \theta_0 + ap + bP$. To take into account a slower increase in θ for the highest values of P, a logarithmic form is introduced, requiring a fourth parameter.

$$\theta = \theta_0 + ap + b\ln(1+cP) \tag{4.5}$$

The four parameters θ_0, a, b, c can be fitted from experimental data by using a simple gradient procedure. The optimisation procedure is summarised in appendix A1.2. The parameters which result from this procedure are θ_0 = -0.1676, a = 0.0168, b = 0.1373, c = 9437.

The result of the optimisation procedure is illustrated on fig. 6, which represents the values of $z = \ln(1+cP)$ as a function of $y = \hat{\theta} - ap$ where $\hat{\theta}$ is the experimental value of θ. According to equ. (4.5), the points should be aligned on a straight line, which is also represented on fig. 6. The approximation is satisfactory, however less accurate for the low values of P.

A more accurate representation of the dilatancy can be obtained but using more than four parameters. The variations of β, drawn as functions of combined deformation p, suggest a representation similar to that of k in section 3.2

$$\beta = \beta_0 + (\beta_m - \beta_0)\left(1 - \frac{1}{1+\beta_1 p + \beta_2 p^2}\right) \tag{4.6}$$

where parameters β_0, β_m, β_1, β_2 must be fitted from the experimental data. These parameters can themselves be defined by four functions of the remaining parameter P to provide an accurate adjustment of the whole dataset. A satisfactory adjustment was obtained with the following four functions

$$\begin{vmatrix} \beta_0 = \beta_{01} + \beta_{02}P + \beta_{03}e^{\beta_{04}P} \\ \beta_1 = \beta_{10} + \beta_{11}e^{\beta_{12}P} \\ \beta_2 = \beta_{20} + \beta_{21}e^{-\beta_{22}P} \\ \beta_m = \beta_{m1} + \beta_{m2}P + \beta_{m3}e^{\beta_{m4}P} \end{vmatrix} \tag{4.7 a,b,c,d}$$

where the involved coefficients are given in Table 1.

The drawback of this procedure is that the global model includes many parameters whose physical

significance is not obvious. On the other hand it matches the experimental data with great accuracy. As a matter of fact in current applications, representation (4.5) may be sufficient.

4.2. Viscoplastic flow rate

The flow rate model below is developed within the framework of the classical additive viscoplasticity (Lemaître and Chaboche, 1994). In that context, the stress tensor can go out of the yield surface so that yield function f takes values greater than 0. Classically a power law expression is used for the plastic strain rate:

$$\dot{\boldsymbol{\varepsilon}}_{\boldsymbol{p}} = \left(\frac{\langle f \rangle_+}{\eta}\right)^N \boldsymbol{n} \tag{4.8}$$

where η is a viscosity parameter, N an appropriate exponent. f is the criterion function as defined by equ. (3.5) and $\boldsymbol{n}$ the plastic flow direction as defined in equ. (4.2). Symbol $\langle f \rangle_+$ stands for the actual value of f, if it is positive, and zero, if it is negative or null.

As this expression is insufficient to represent the viscous response of the material, an exponential expression can be used (Lemaitre and Chaboche, 1994): $\dot{\boldsymbol{\varepsilon}}_{\boldsymbol{p}} = \left(\frac{\langle f \rangle}{\eta}\right)^N e^{\alpha f^{N+1}} \boldsymbol{n}$ (4.9)

Dilatancy β can be recovered from equ. (4.2):

$$\dot{\boldsymbol{\varepsilon}}_{\boldsymbol{p}} = \frac{1}{\sqrt{3(1+\beta^2)}}\left(\frac{\langle f \rangle}{\eta}\right)^N e^{\alpha f^{N+1}} \left(\frac{\boldsymbol{\sigma^D}}{\tau} + \beta \mathrm{I}\right) \tag{4.10}$$

To fit the three parameters η, N, α only the stress variation during the last relaxation phase is used (fig. 7). The reason is that all along this phase, maximum hardening is reached and - as strain is almost constant - damage can also be assumed as constant. As a result the longitudinal plastic strain rate is simply: $\dot{\varepsilon}_p = -\frac{\dot{\sigma}}{E}$, E being Young's modulus. For each test the last relaxation curve thus provides a sequence of stress values σ and corresponding strain rates $\dot{\varepsilon}_p$. The associated criterion values f are computed from equ. (3.5), so that a series of curves $(f, \dot{\varepsilon}_p)$ can be drawn (fig. 8). The three parameters η, N, α are then fitted through an optimisation procedure. Details on the method are given in appendix A1.3. The following parameters are obtained: $N = 1$, $\alpha = 1.62$, η = 1.36d6.

4.3. Isotropic damage modelling

Assuming isotropic damage, experimental data shows that the phenomenon regularly increases according to the highest positive principal strain $\left\langle \varepsilon_I \right\rangle_+^{\max}$ (Mazars, 1981). This hypothesis is an expression of a probable damage mechanism resulting from the development of internal micro-cavities with tensile efforts.

A damage factor d is classically defined as: $$d = \frac{E_0 - E}{E_0} \qquad (4.11)$$

so that damage has a direct effect on elastic modulus E_0. Elastic Poisson's ratio ν is set to a constant value 0.3.

The behaviour rule can be expressed in an incremental form (Ladevèze et al, 2000)

$$\dot{d} = \frac{1}{\tau_c}\left[1 - e^{\left(-a\left\langle d^s - d\right\rangle\right)}\right] \text{ if d < 1 otherwise, d = 1} \qquad (4.12\text{ a})$$

A hyperbolic form is sufficient to reproduce approximately the evolution of the damage factor, its value being bounded to 1:

$$d^s = \min\left[1\ ,\ \left(d_1 + d_2 \sup_t \left\langle \varepsilon_I \right\rangle_+^{\max}\right)\left(1 - \frac{1}{1 + d_3 \sup_t \left\langle \varepsilon_I \right\rangle_+^{\max}}\right)\right] \qquad (4.12\text{ b})$$

which implies that for low damage rates, $d = d^s$. In this equation, symbol $\sup_t \langle . \rangle$ indicates the highest value of a variable during the test. Symbol d^s instead of d in (4.12 b) is emphasised to differentiate "static damage" from "delayed damage" (4.12 a). The latter takes into account the viscous part of damage. However, this part is assumed to be weak so that it can be neglected during the characterisation step. The parameter identification is thus performed by assuming $d = d^s$ according to eq. (4.12 b), thus using instantaneous damage instead of viscous damage. Conversely, the incremental model (4.12 a) is implemented into the numerical model. From the simulations it turned out that the viscous part of damage remains negligeable up to the collapse point during the loading phase, but more important after.

Once more, the hyperbolic form (4.12 b) is chosen for its ability to reproduce, at least roughly, the shape of the experimental results. This curve monotonously increases with strain up to the obvious asymptotic limit of 1.

The experimental values of d immediately result from the measurements of E and equ. (4.11). The

corresponding values of $\langle \varepsilon_I \rangle_+^{\max}$ result from the knowledge of the current strain tensor at the experimental points. Coefficients d_1, d_2, d_3 in equ. (4.12 b) are determined through an optimisation procedure. As the phenomenon is mainly governed by local tensile effects, the tensile curves are given a double weight in the optimisation process. Details on the method are given in appendix A1.4. Figure 9 shows the damage curves resulting from the model above, together with the experimental values.

As a matter of fact, the transverse strain curves (fig. 2) allow a similar characterisation of damage. Unfortunately, the result obtained is somewhat different from the previous one. This proves that damage is not really isotropic and would require a more complex model. A model with non isotropic damage would probably improve the coherence of the model. Actually, this discrepancy has not been resolved and transverse deformations have not been considered in the damage model.

5. Computational applications

5.1. Simulation tests

The model can be considered a satisfactory if it can to reproduce a complex loading-unloading cycle. To perform this simulation, the complete model is implemented into computer code ABAQUS as a UMAT subroutine.

Figures 10, 11, 12 show the simulations of three loading programs: a cyclic uniaxial compressive test, a cyclic compressive test with a 10 MPa hydrostatic pressure and a cyclic tensile test. The pressure effect is correctly reproduced. The relaxed points are reached for all the three tests. The viscous stress is slightly underestimated for high pressures. The plastic strains are correctly reproduced, but the viscous effects observed on the experimental unloading-loading cycles are not. Recent experimental tests including significant recovery phases and also recent dynamic tests (DMA) reveal the visco-elasticity of the material. Due to the isotropic damage hypothesis, the damage evolution law is an average of the longitudinal and tranverse experimental damage levels. It results in overestimating the longitudinal damage and underestimating the transverse one, as can be seen on the unloading-loading cycles. Thereby, the lateral strain is somewhat underestimated, especially for the last cycles.

5.2. Sensitivity analysis

To get a better understanding of the hierarchical effects of these 30 parameters on the model response, a sensitivity analysis is performed by means of a perturbation method. The reponses derived from uniaxial tensile, uniaxial compressive, triaxial compressive (up to 10 MPa) simulations, while cancelling the rupture criterion, are analysed. The loading rate is set to 3.3 10^{-5} s^{-1}. Each simulation is carried up to its corresponding experimental level, i.e. is 0.14% under an uniaxial tension, 1.55 % under an uniaxial compression and 2.7 % under a triaxial compression.

From the identified parameter set, a 1% perturbation is applied to each parameter to perform a new series of simulation. The difference between the reference solution $(\sigma^{ref}, \varepsilon^{ref})$ and a perturbed sulution $(\sigma^{pert}, \varepsilon^{pert})$ is quantified as follows:

$$s = \sum_{\substack{\text{Longitudinal} \\ \text{\& transversal} \\ \text{responses}}} \sum_{\substack{\text{Tensile,} \\ \text{compressive and} \\ \text{confined test}}} \frac{\int_{\substack{\text{Time} \\ \text{test}}} \left\{ \left(\sigma^{ref}(t) - \sigma^{pert}(t) \right) \dot{\varepsilon}^{ref}(t) - \left(\varepsilon^{ref}(t) - \varepsilon^{pert}(t) \right) \dot{\sigma}^{ref}(t) \right\} dt}{\int_{\substack{\text{Time} \\ \text{test}}} \sigma^{ref}(t) \dot{\varepsilon}^{ref}(t) dt} \times 100\ \%$$

The results are presented on fig. 13. On the left diagram, parameter sensitivities have been summed by groups associated with the 5 fundamental mechanisms. The results show that the elastic parameters and those of the yield surface have a major role in the model. The damage parameters represent an important part too, with a sensitivity factor of around 13%. The viscous parameters - despite a supposed rather low strain rate - and the flow rule parameters stand at around a 5% sensitivity value, which is lower, yet not negligeable.

More detailed results are presented on the right diagram, by groups corresponding to the different mechanisms. It results that only one damage parameter c_1, and 4 dilatancy parameters have a sensitivity below 1% on the model response. This explains why a simplified formulation of the dilatancy could be proposed in section 4.1 with a rather small loss of accuracy.

6. Conclusion

The development of the model has required to consider – even roughly – at least five essential material features : plasticity, hydrostatic pressure sensitivity, strain-hardening, non-associated flow rule and damage. Globally, the model provides a satisfactory representation under complex loading programs, despite the width of the application field: tensile, compressive, tri-axial, monotonous or cyclic loading paths,

proportional or not.

Actually, the construction of the yield curves and the adjustment of the hardening law have been more carefully developed, since they are the skeleton of the model. Although tensile curves are truncated by early fracture, they could be used as well as compressive curves for the model to reproduce any tensile and compressive loading path.

Modelling the flow direction and the flow rate entails more rough approximations. The comparison with experimental data shows a satisfactory correlation for the dilatancy.

Globally, the model describes relatively well the strengthening effect of the hydrostatic pressure. On the other hand the visco-plastic behaviour could be improved, and the visco-elastic effects should be usefully introduced. Moreover, considering the flow rate as a function of unique yield criterion *f* is probably a coarse hypothesis, as shown by the great dispersion of the experimental results. A consistent visco-plastic formulation, as was recently proposed (Winnicki and al, 2001), could be a route towards a real improvement of the model.

Furthermore, damage modelling is the source of specific difficulties. Damage is apparently hydrostatic-pressure-dependent. To take this effect into account, some authors (Hackett and Bennett, 2000) have recently modified a crack growth law proposed in literature (Dienes and Kershner, 1998). They developed a new formulation of damage by taking into account the hydrostatic pressure dependency and the difference between tensile and compressive responses - in terms of mean pressure sign -. Actually, considering the unilateral closing/unclosing effects of the cracks observed in the non-proportional tests, it should be preferable to distinguish the presence of damage from its effects. For this kind of energetic material, damage is generally modeled as isotropic. In the present model, the anisotropic effect is neglected because of the great complexity of the model. The simulation betrays this problem as the lateral deformation is effectively underestimated. To introduce this anisotropy, a solution has recently been proposed (Dienes et al, 2006). Some anisotropy of the crack distribution is taken into account as well as coalescence and nucleation of cracks. Independently, another approach is initiated by some authors (Denoual and Hild, 2000) to improve the damage description. It is assumed that a damage tensor depending on three independent scalar variables matches the principal stress frame. Finally, a somewhat different approach introducing micro-planes to better describe the plastic behaviour (Carol and Bazant, 1997), the pressure effects (Stephen and Foster, 2000), and the anisotropy (Wu and Li, 2008) could present promising perspectives.

Beyond the present study, three phenomena highly relevant to the present material have not be

considered: the impact of the temperature on the mechanical characteristics, the visco-elastic behaviour and the fracture bounds. These issues are currently being investigated by the authors.

Appendix

A1. Parameter optimisation procedures

A1.1. Optimisation of the yield curve parameters

The purpose is to fit the 5 parameters X_0, k_0, δ, c_1, c_2 which define the yield curves through equ. (3.5), (3.6). The criterion of optimality is defined as the sum of the distances of the experimental points to the mean curve defined by equ. (3.10):

$$J = \sum_{i=1,N} \left(\hat{k}_i - k_i \right)^2 \qquad \text{(A1.1)}$$

In this equation, k_i is the strain-hardening parameter obtained at any experimental point (i) by solving equ. (3.5), $\hat{k}_i$ is the estimate of the same quantity obtained from equ. (3.8) and (3.10), and N is the total number of experimental points.

From an initial solution q_0, an optimal solution q_1 is determined in the opposite direction of gradient vector: $v_1 = -J'^T(q_0)$, then the same procedure is applied to find a better solution q_2, etc. The procedure is stopped when function J does not decrease more than a defined small value ε_J. Initial solution q_0 is found by heuristic manipulation. It turns out that an optimal solution is obtained after 29 iterations for $\varepsilon_J = 10^{-4}$, so that a more advanced method is not required.

A1.2. Dilatancy parameter optimisation

The purpose is to fit the four parameters θ_0, a, b, c which define the flow direction by equ. (4.5). Once more an error function J of parameter vector $q = \left[\theta_0, a, b, c \right]^T$ is defined as the mean squared error between the real values and their estimates:

$$J(q) = \sum_{i=1,N} (\hat{\theta}_i - \theta_i)^2$$

where $\hat{\theta}_i$ is the experimental value of θ at point (i), according to equ. (4.4), and θ_i its estimate from equ. (4.5). At each step a "better"parameter vector $q_{n+1} = q_n + \rho v_{n+1}$ is searched in the opposite direction of the current gradient: $v_{n+1} = -J'^T(q_n)$ until function J does not move more than a given value ε_J.

From gradient expression (A1.3), and taking equ. (4.5) into account, direction v is the transposed vector of $J'(q) = \left[1 \quad p \quad \ln(1+cP) \quad \frac{bp}{1+cP} \right]$

A small increment size ρ is taken so as to obtain an accurate adjustement is obtained. Starting from an initial solution q_0 found by heuristic manipulation, and using an increment size of 5.10^{-4} for $\varepsilon_J = 10^{-4}$ an optimised solution is obtained after 213 iterations.

A1.3. Optimisation of the flow rate parameters

The purpose is to fit coefficients η, N, α which define the flow rate modulus in equ. (4.10). Writing this equation in the logarithmic form:

$$\ln(\dot{\varepsilon}_p) = N\left[\ln < f > -\ln(\eta)\right] + \alpha < f >^{N+1} \qquad \text{(A1.2)}$$

coefficient N appears as the slope of the asymptot of $y = \ln(\dot{\varepsilon}_p)$ as a function of x=ln<f> , for $< f > \to \infty$. A mean value of this slope is easily identified on diagrams $y(x)$. The other unknowns in (A1.6): $Log(\eta)$ and α, are then identified as the least squares solution to the overdetermined system:

$$\alpha < f_i >^{N+1} - N\ln(\eta) = \ln(\dot{\varepsilon}_p)_i - N\ln < f_i >$$

extended to the set of pairs $\left(\ln(\dot{\varepsilon}_p)_i, < f_i >\right)$ available at N experimental points i=1,N.

A1.4. Optimisation of the damage parameters

The purpose is to fit coefficients d_1, d_2, d_3, which define the damage model (4.12). Writing this equation in the form: $(d_1 d_3)\sup_t \langle \varepsilon_I \rangle_+^{\max} + (d_2 d_3)\left(\sup_t \langle \varepsilon_I \rangle_+^{\max}\right)^2 - d_3\left(d \sup_t \langle \varepsilon_I \rangle_+^{\max}\right) = d$

for every experimental pair $\left(\sup_t \langle \varepsilon_I \rangle_+^{\max}, d\right)$, the least squares method is applied to obtain coefficients a=$d_1 d_3$, b=$d_2 d_3$, c= d_3 . Coefficients d_1, d_2, d_3 result directly from a, b, c.

A2. Expression of the plastic strain rate

The purpose is to link the plastic flow direction $\boldsymbol{n}$ with dilatancy β.

From properties $\frac{\partial \tau}{\partial \boldsymbol{\sigma}} = \frac{\boldsymbol{\sigma}^{\mathbf{D}}}{3\tau}$ and $\frac{\partial P}{\partial \boldsymbol{\sigma}} = \frac{\mathbf{I}}{3}$ the flow rule is:

$$\dot{\boldsymbol{\varepsilon}}_{\mathbf{p}} = \dot{\lambda}\left(\frac{\partial g(\tau,P)}{\partial \tau}\frac{\partial \tau}{\partial \boldsymbol{\sigma}} + \frac{\partial g(\tau,P)}{\partial P}\frac{\partial P}{\partial \boldsymbol{\sigma}}\right) = \frac{\dot{\lambda}}{3}\left(\frac{\partial g(\tau,P)}{\partial \tau}\frac{\boldsymbol{\sigma}^{\boldsymbol{D}}}{\tau} + \frac{\partial g(\tau,P)}{\partial P}\mathbf{I}\right) \qquad \text{(A2.1)}$$

hence $\varepsilon_p^v = Tr(\dot{\boldsymbol{\varepsilon}}_{\mathbf{p}}) = \dot{\lambda}\dfrac{\partial g}{\partial P}$ and $\dot{\boldsymbol{\varepsilon}}_{\boldsymbol{p}}^{\boldsymbol{D}} = \dot{\boldsymbol{\varepsilon}}_{\mathbf{p}} - \dfrac{1}{3}Tr(\dot{\boldsymbol{\varepsilon}}_{\mathbf{p}})\mathbf{I}$

It results that: $$\dot{\varepsilon}_p^D = \sqrt{3\dot{\varepsilon}_p^D : \dot{\varepsilon}_p^D} = \dot{\lambda}\frac{\partial g(\tau,P)}{\partial \tau} \qquad \text{(A2.2)}$$

Using the definition of dilatancy β: $$\frac{\partial g(\tau,P)}{\partial P} = \beta\frac{\partial g(\tau,P)}{\partial \tau} \qquad \text{(A2.3)}$$

and equ. (A2.2) the flow tensor (A2.1) becomes: $\dot{\boldsymbol{\varepsilon}}_{\boldsymbol{p}} = \dot{\lambda}\dfrac{\partial g(\tau,P)}{\partial \tau}\left(\dfrac{\boldsymbol{\sigma}^D}{3\tau} + \beta\dfrac{\mathbf{I}}{3}\right) = \dot{\lambda}\boldsymbol{n}$

The normalised flow direction $\boldsymbol{n}$ is such that $\boldsymbol{n} : \boldsymbol{n} = 1$, which gives: $\dfrac{\partial g(\tau,P)}{\partial \tau} = \sqrt{\dfrac{3}{1+\beta^2}}$

$$\dot{\boldsymbol{\varepsilon}}_{\boldsymbol{p}} = \frac{1}{\sqrt{3(1+\beta^2)}}\left(\frac{\langle f \rangle}{\eta}\right)^N e^{\alpha f^{N+1}}\left(\frac{\boldsymbol{\sigma}^D}{\tau} + \beta\mathbf{I}\right)$$

Références

[1] Wiegand D.A., 1999, The influence of confinement on the mechanical properties of energetic materials, Shock Compression Condensed Matter, eds. M.D. Furnish, L.C. Chhabildas, R.S. Hixson, AIP.

[2] Wiegand D.A., 2003, Reddingius B, Mechanical properties of plastic bonded composites as a function of hydrostatic pressure, Shock Compression Condensed Matter, eds. M.D. Furnish, Y.M. Gupta, J.W. Forbes, AIP.

[3] Funk D.J., Laabs G.W., Peterson P.D., Asay B.W., 1995, Measurement of the stress/strain response of energetic materials as a function of strain rate and temperature: PBX9501 and mock 9501, Shock Compressed Condensed Matter APS, Seattle (USA),

[4] Idar D.J., Thompson D.G., Gray III G.T., Blumenthal W.R., Cady C.M., Peterson P.D., Roemer E.L., Wright W.J., Jacquez B.L., 2001, Influence of the polymer molecular weight, temperature and strain rate on the mechanical properties of PBX 9501. Shock Compression Condensed Matter, ed Furnish/Thadhani/Horie AIP.

[5] Addessio F.L., Johnson J.N., 1990, A constitutive model for the dynamic response of brittle materials, J. Appl. Phys. 67, pp 3275-3286.

[6] Bennett J.G., Haberman K.S., Johnson J.N., Asay B.W., Henson B.F., 1998, A constitutive model for the non-shock ignition and mechanical response on high explosives, J. Mech. Phys. Solids, 46 (12), pp 2303-2322.

[7] Hackett R.M., Bennett J.G., 2000, An implicit finite element material model for energetic particulate composite materials, Int. J. Numer. Meth. Eng., 49 (12), pp 1191-1209.

[8] Aubertin M., Li L., 2004, A porosity-dependent inelastic criterion for engineering materials, Int. J. of

Plasticity 20, pp 2179-2208.

[9] Prevost J.H., Popescu R., 1996, Constitutive Relations for Soil Materials, Electronic Journal of Geotechnical Engineering, Premiere Issue.

[10] Coussy O, 1995, Mechanics of Porous Continua, John Wiley & Sons Ed..

[11] Gontier C., Bouchou A., Vinot C., 2001, An anisotropic mechanical model of a phenolic foam in compression , Int. J. of Mechanical Sciences, 43, pp 2371-2384.

[12] Hicher P.Y.& Shao J.-F., 2008, Constitutive Modeling of Soils and Rocks, Wiley Ed..

[13] Schleicher F., Angew Z., 1996, Math. Mech., pp 166-199.

[14] Drucker D.C., Asce A.M., Gibson R.E. & Henkel D.J., 1957, Soil Mechanics and Work-hardening theories of plasticity, Trans. American Society of Civil Engineers, 122.

[15] Pan X.D., Hudson J.A., 1988, A simplified three dimensional Hoek-Brown yield criterion, Rock. Mechanics and Power Plants, M. Romana Ed., Balkema Rotterdam, pp 95-103.

[16] Raghava R., Caddekk R.M. & Yeh G.S.Y., 1973, The macroscopic yield behaviour of polymers, J. Material Science, 8, pp 225-232.

[17] Winnicki A., Paerce C.J., Bicanic N., 2001, Viscoplastic Hoffman consistency model for concrete, Computers and Structures, pp 7-19.

[18] Shao J.F., Jia Y., Kondo D. and Chiarelli A.S.,March 2006, A coupled elastoplastic damage model for semi-brittle materials and extension to unsaturated conditions, Mechanics of Materials, Vol. 38, Iss. 3, pp 218-232.

[19] Nova R., 1982, A model of soil behaviour in plastic and hysteretic ranges, Proc. International Workshop on Constitutive Behaviour of Soils, Grenoble, France, pp 289-309.

[20] Lemaitre J., Chaboche J.-L., 1994, Mechanics of solid materials, Cambridge University Press.

[21] Mazars J., 1981, Mechanical damage and fracture of concrete structure, Proc. 5th Int. Conf on Fracture, Cannes, France, pp 1499-1506.

[22] Ladevèze P., Allix O., Deü J.-F., Lévêque D., 2000, A mesomodel for localisation and damage computation in laminates, Computer Methods in Applied Mechanics and Engineering, Vol. 183, Iss. 1-2, pp 105-122.

[23] Dienes J.K., Kershner J.D.,1998, Multiple shock initiation via statistical crack mechanics, 11th Int. Symp. Detonation, Snowmass (USA).

[24] Dienes J.K., Zuo Q.H., Kershner J.D., 2006, Impact initiation of explosives and propellants via statistical crack mechanics, J. Mech. Phys. Solids, Vol. 54, pp 1237-1275.

[25] Carol I., Bazant Z. P., 1997, Damage and plasticity in microplane theory, Int. J. Solids Structures, Vol. 34, n°29, pp 3807-3835.

[26] Stephen J. L., Foster J., 2000, A three-dimensional finite element model for confined concrete structures, Computers and structures, Vol. 77, pp 441-451.

[27] Wu J.-Y., Li J., 2008, On the mathematical and thermodynamical descriptions of strain equivalence based anisotropic damage model, Mechanics of Materials,vol 40, pp 377-400.

[28] Denoual C., Hild F., 2000, A damage model for the dynamic fragmentation of brittlesolids, Comput. Methods Appl. Mech. Engrg., Vol. 183, pp 247-258.

FIGURE CAPTIONS

Fig. 1. Three examples of cyclic loading tests. Both longitudinal and lateral strains are represented. Bold line: pure longitudinal compressive test; thin line: compressive test with a 10 MPa initial hydrostatic pressure; up left: zoom on a tensile loading path.

Fig. 2. Cyclic compressive test with a 5 MPa hydrostatic pressure. Bold line: a typical loading-unloading cycle. Dot-point line $C_iA_{i+1}G_{i+1}$ indicates the elastic unloading path. B_nC_n represents the last relaxation phase. R is the rupture point.

Fig. 3. Experimental points on (P ,τ) plane. Thin line: approximation of a current yield curve by a parabola. Bold dashed line: extreme yield curve. Narrow band between dashed lines: probable position of the initial yield curve. Top right: meaning of the yield curve adjustment parameters.

Fig. 4. Optimisation of the strain-hardening law. Thin lines: experimental paths; bold line: optimal (k,p) curve.

Fig. 5. Yield parabolas according to the strain-hardening model. The arrows represent the real flow directions at the experimental points.

Fig 6. Optimisation of the dilatancy parameters : $z = \ln(1 + cP)$ vs $y = \hat{\theta} - ap$. Experimental points. Straight line: model approximation.

Fig. 7. A typical relaxation curve

Fig. 8. Optimisation of viscoplastic flow law. Experimental points and model.

Fig. 9. Damage parameter optimisation.

Fig. 10. Simulation of cyclic compressive test without hydrostatic pressure.

Fig. 11. Simulation of cyclic compressive test with a 10 MPa hydrostatic pressure

Fig. 12. Simulation of a cyclic tensile test

Fig. 13. Global sensitivity of the mechanisms in the model, and parameters sensitivity relative to each mechanism

TABLE

β_0	β_m	β_1	β_2
β_{01} = -0,11	β_{m1} = 0,476	β_{11} = 180	β_{21} = 37
β_{02} = 6,38.10^{-3}	β_{m2} = 0,01377	β_{12} = 450	β_{22} = 33
β_{03} = 0,12	β_{m3} = 0,039	β_{13} =0,18	β_{23}=0,318
β_{04} = 1,598	β_{m4} = 1,94		

Table 1. Optimisation of the dilatancy model: coefficients of the accurate model. (4.3)-(4.4)

FIGURES

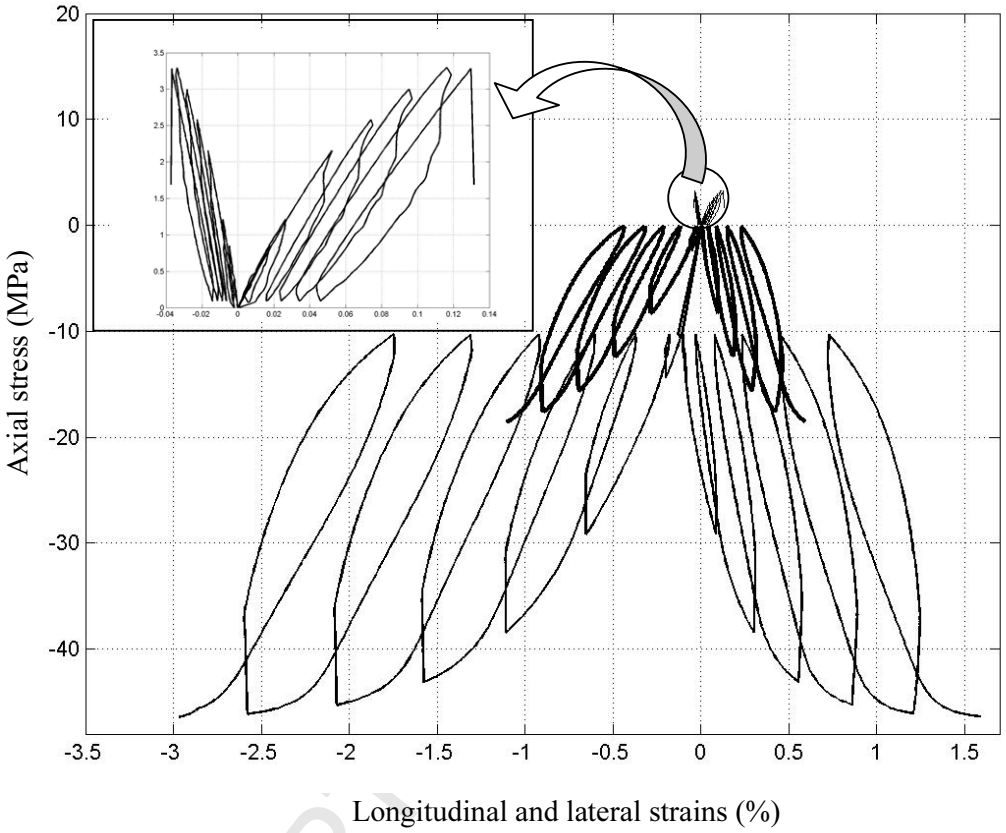

Fig. 1. Three examples of cyclic loading tests. Both longitudinal and lateral strains are represented. Bold line: pure longitudinal compressive test; thin line: compressive test with a 10 MPa initial hydrostatic pressure; up left: zoom on a tensile loading path.

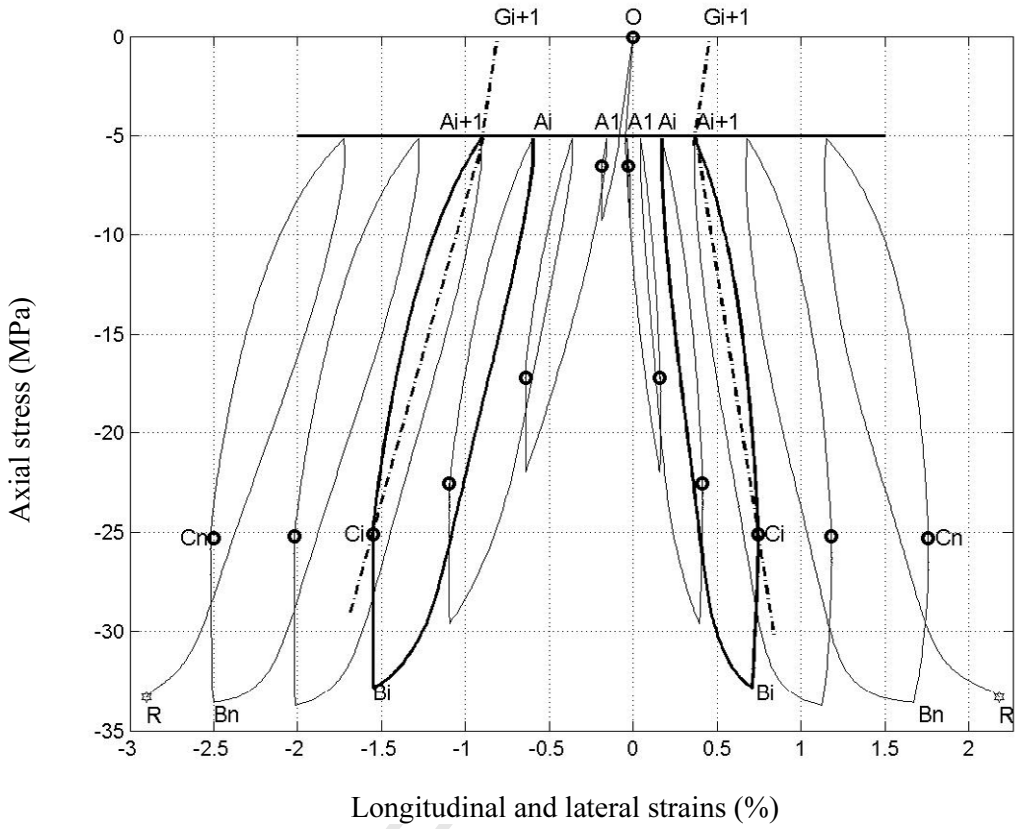

Fig. 2. Cyclic compressive test with a 5 MPa hydrostatic pressure. Bold line: a typical loading-unloading cycle. Dot-point line $C_iA_{i+1}G_{i+1}$ indicates the elastic unloading path. B_nC_n represents the last relaxation phase. R is the rupture point.

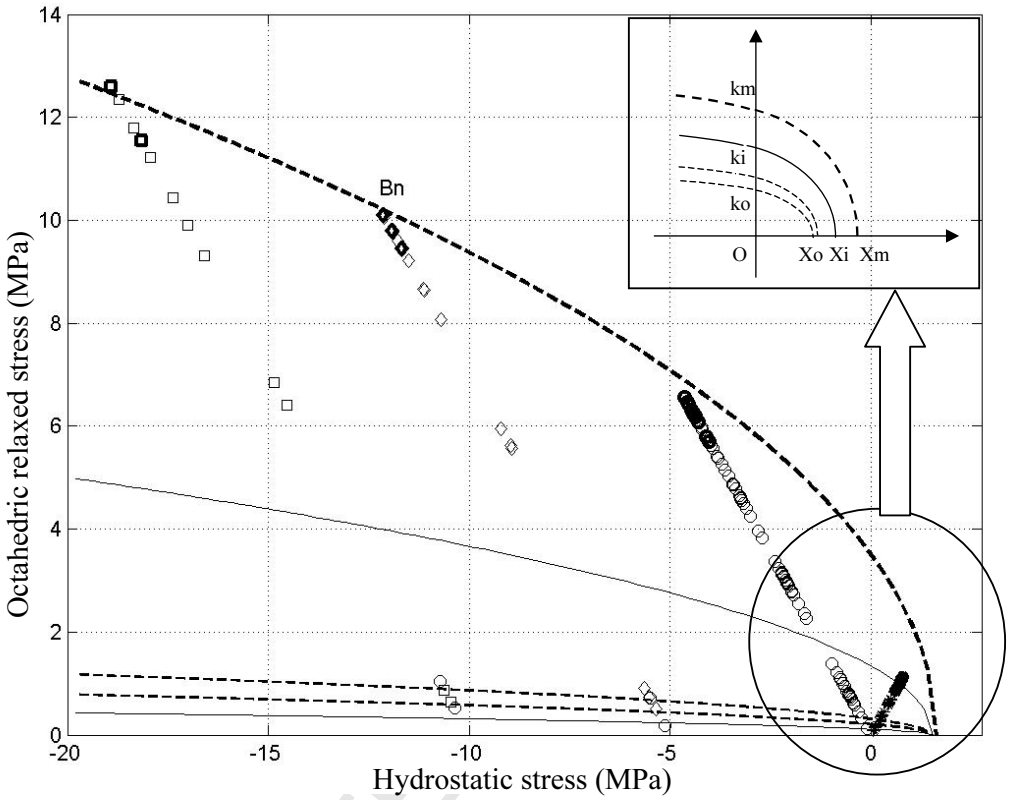

Fig. 3. Experimental points in (P,τ) plane. Thin line: approximation of a current yield curve by a parabola. Bold dashed line: extreme yield curve. Zone between thin dashed lines: likely position of the initial yield curve. Up right: meaning of the yield curve adjustment parameters.

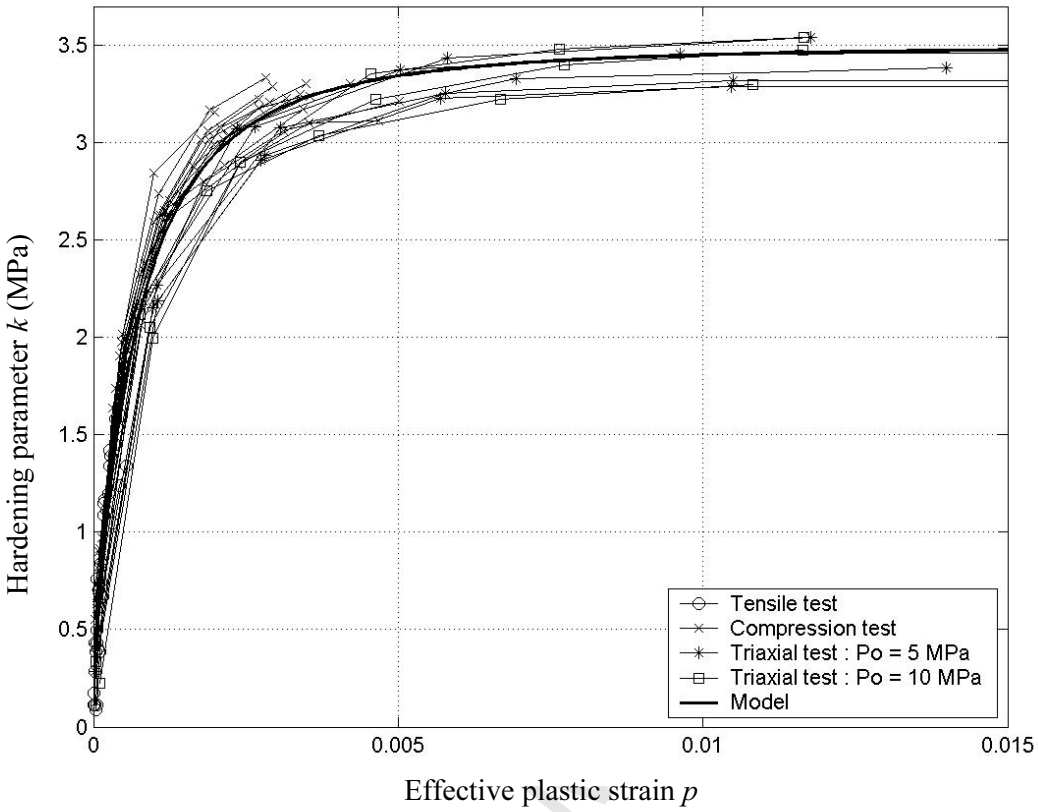

Fig. 4. Optimisation of the strain-hardening law. Thin lines: experimental paths; bold line: optimal (k,p) curve.

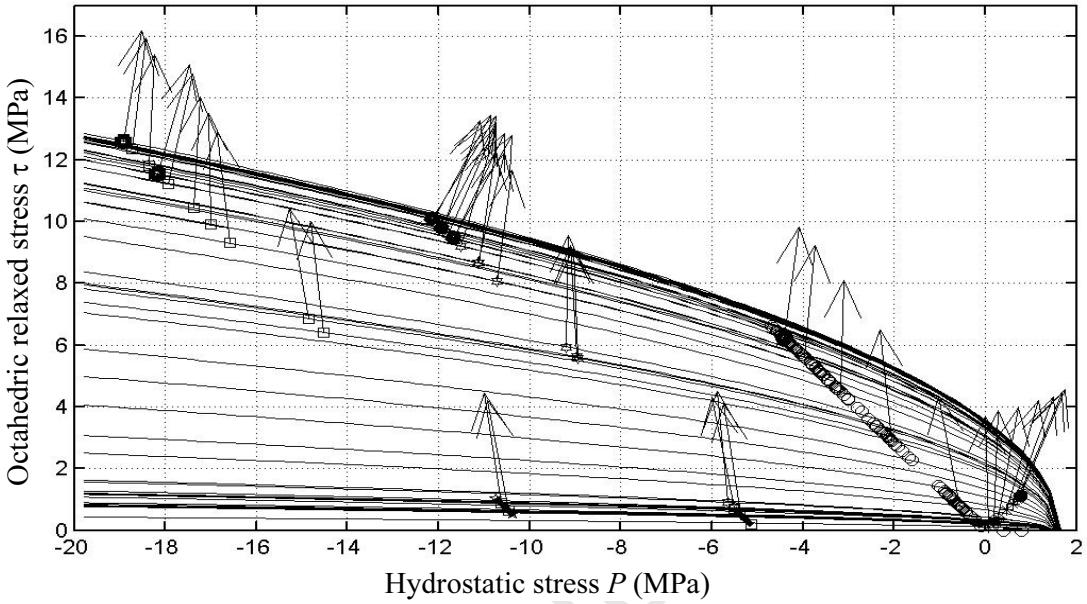

Fig. 5. Yield parabolas according to strain-hardening model. The arrows represent the real flow directions at the experimental points.

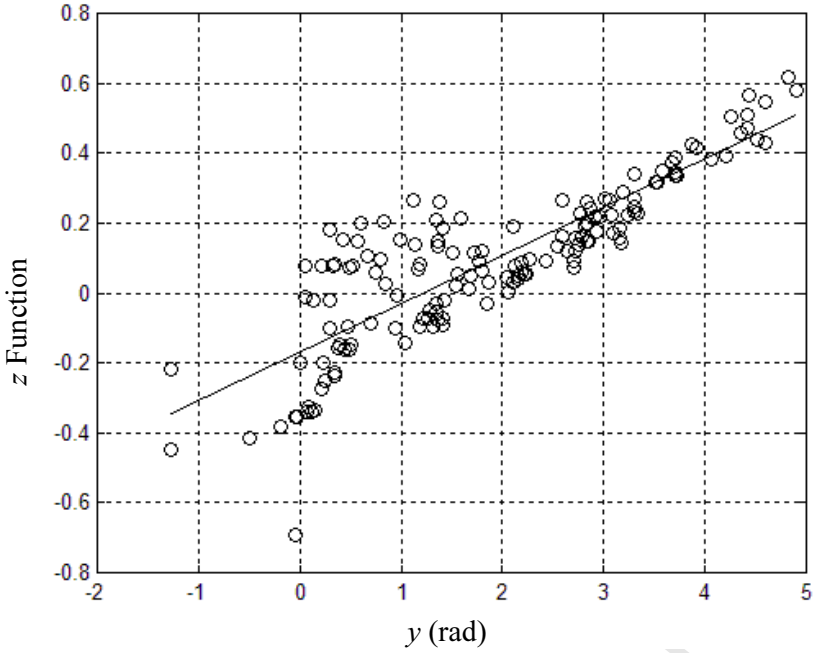

Fig 6. Optimisation of the dilatancy parameters : $z = \ln(1+cP)$ *vs* $y = \hat{\theta} - ap$. Experimental points. Straight line: model approximation.

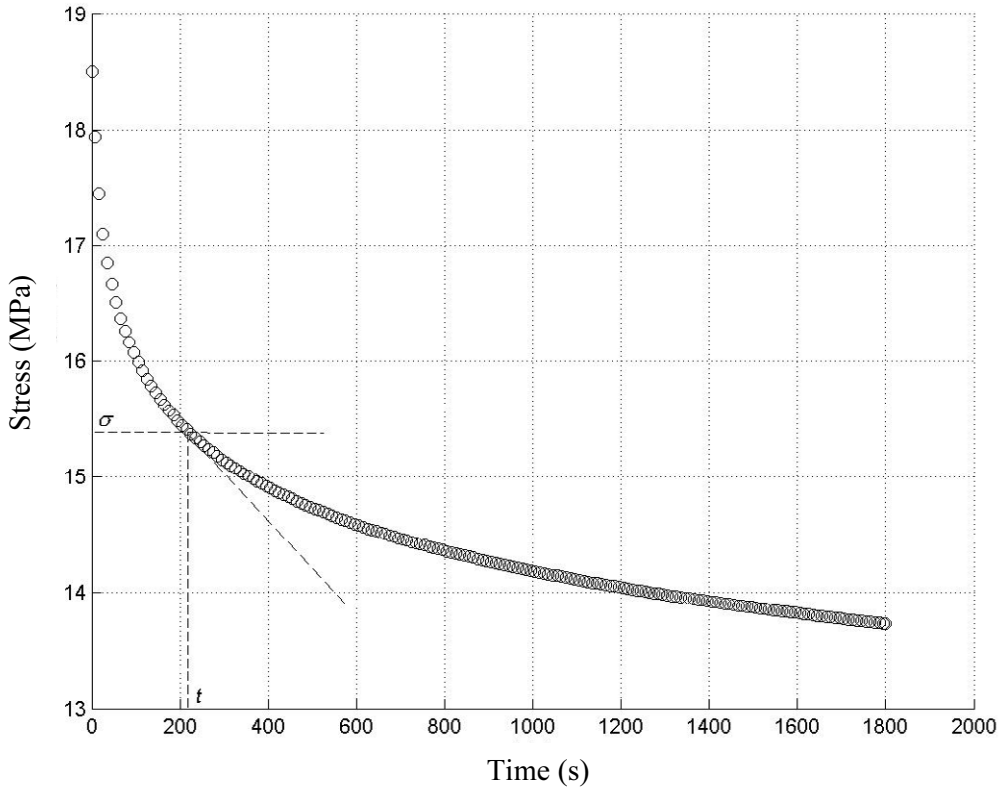

Fig. 7. A typical relaxation curve

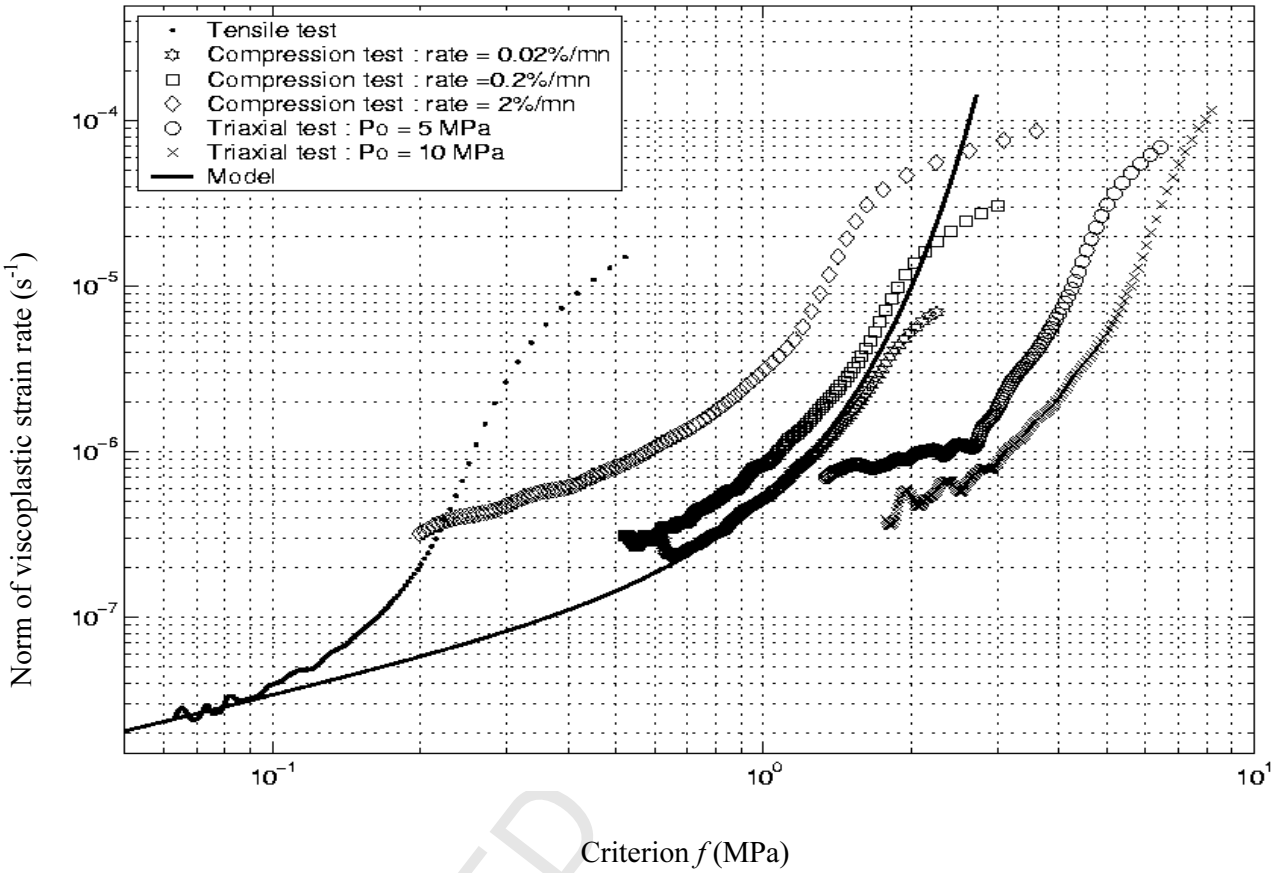

Fig. 8. Optimisation of viscoplastic flow law. Experimental points and model.

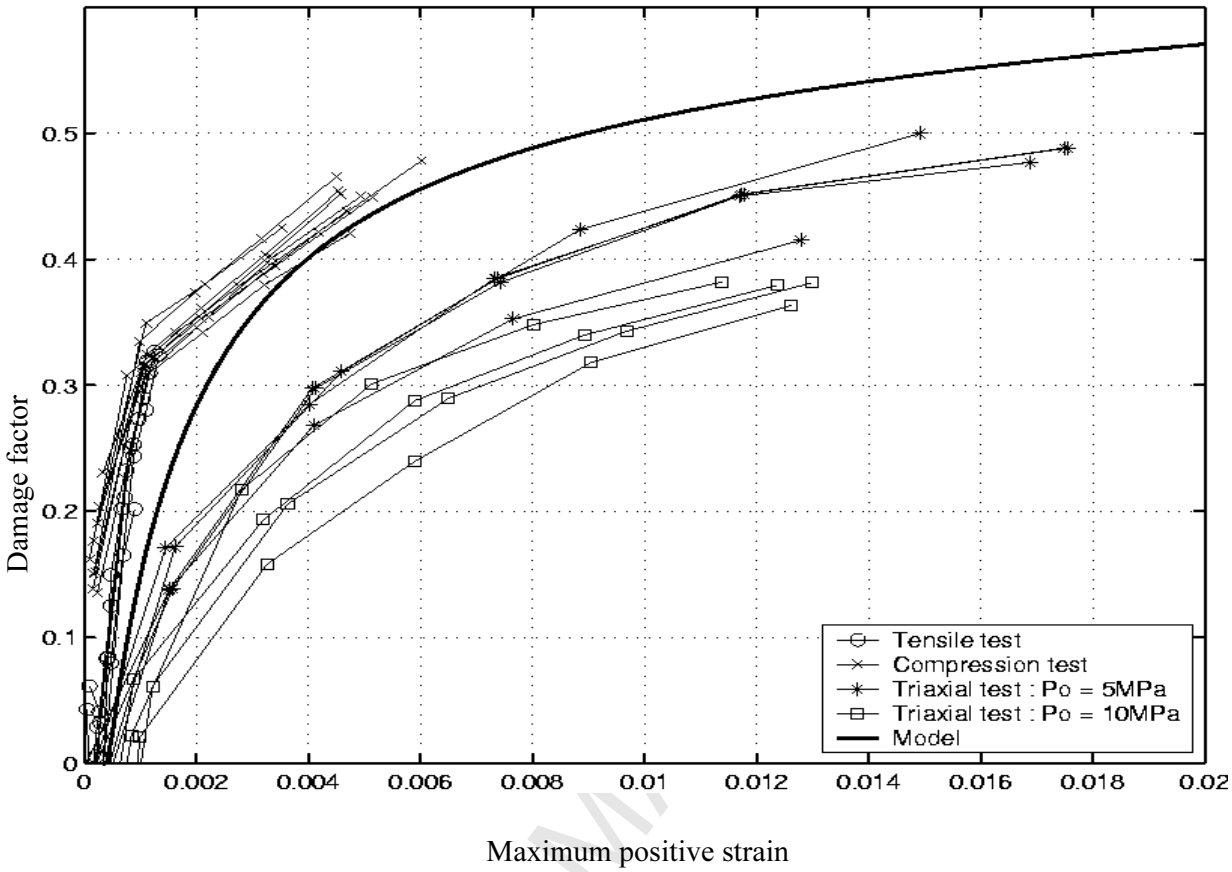

Fig. 9. Damage parameter optimisation.

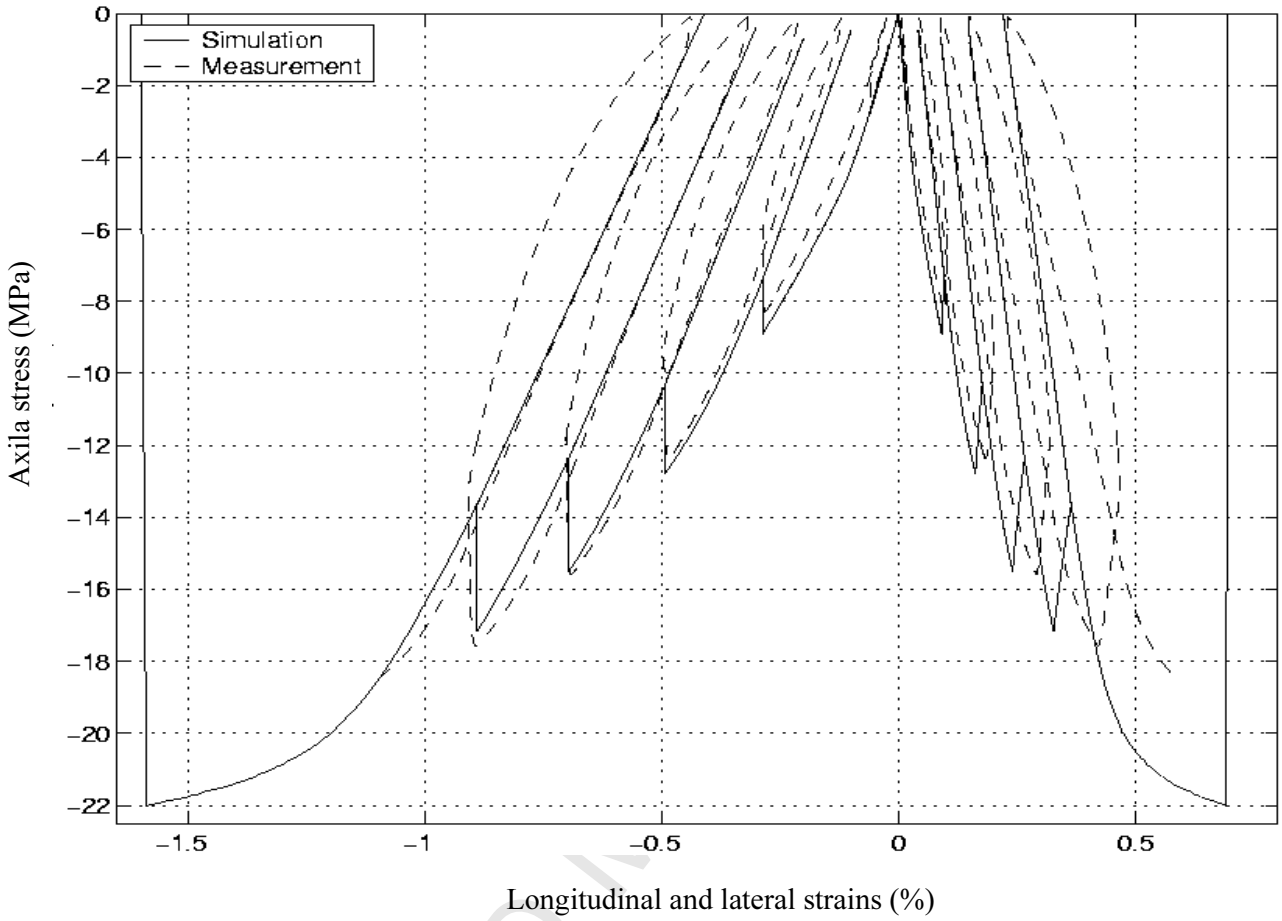

Fig. 10. Simulation of cyclic compressive test without hydrostatic pressure.

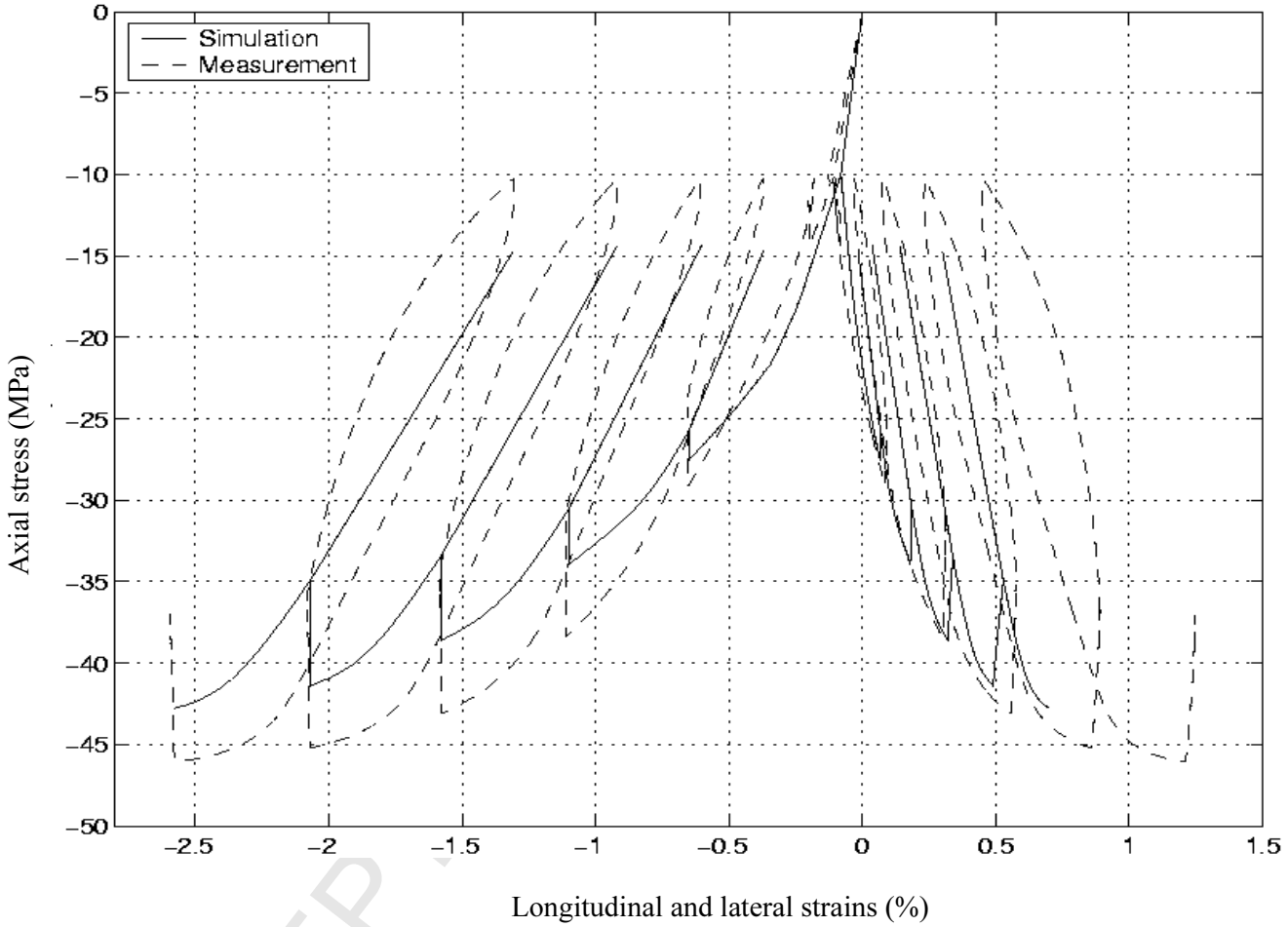

Fig. 11. Simulation of cyclic compressive test with a 10 MPa hydrostatic pressure

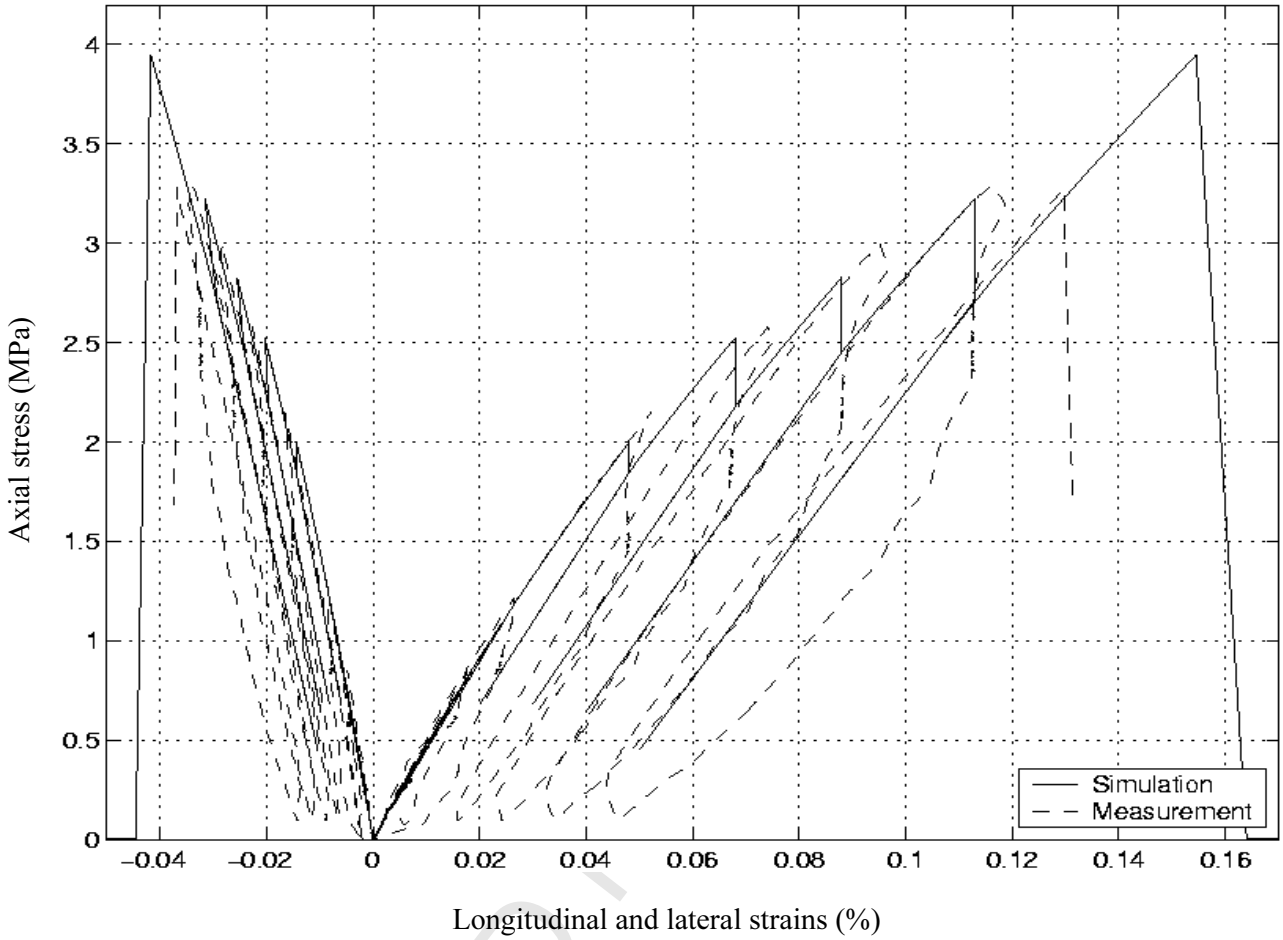

Fig. 12. Simulation of a cyclic tensile test

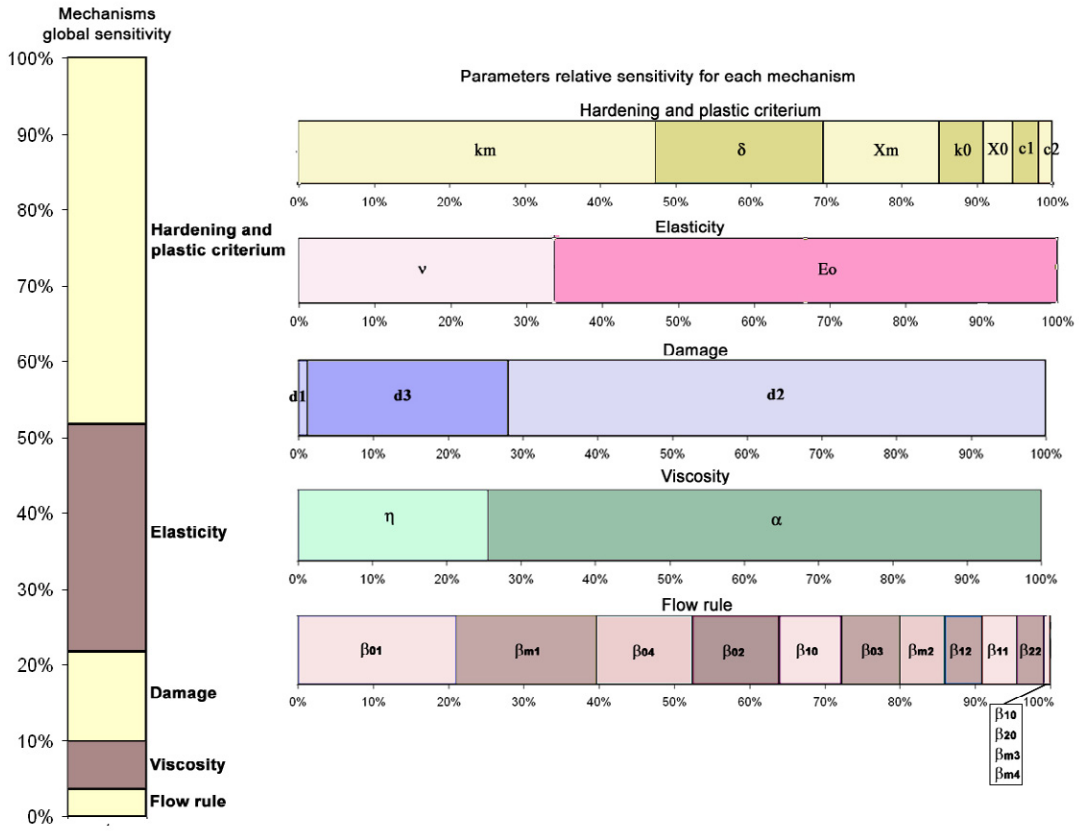

Fig. 13 : Global sensitivity of the mechanisms in the model, and parameters sensitivity relative to each mechanism